Lab on a Chip

A point-of-care microfluidic biosensing system for rapid and ultrasensitive nucleic acid detection from clinical samples

Journal:	*Lab on a Chip*
Manuscript ID	LC-ART-04-2023-000372.R1
Article Type:	Paper
Date Submitted by the Author:	08-Jun-2023

Complete List of Authors:	Zhang, Yuxuan; University of Connecticut Song, Yang; University of Connecticut Weng, Zhengyan; University of Connecticut Yang, Jie; Rice University Avery, Lori; UConn Health Dieckhaus, Kevin; UConn Health Lai, Rebecca Y.; University of Nebraska-Lincoln Gao, Xue; Rice University, Zhang, Yi; University of Connecticut, Biomedical Engineering

A point-of-care microfluidic biosensing system for rapid and ultrasensitive nucleic acid detection from clinical samples

Yuxuan Zhang[1,2†], Yang Song[1,2†], Zhengyan Weng[1,2], Jie Yang[3,#], Lori Avery[4], Kevin D. Dieckhaus[5], Rebecca Y. Lai[6], Xue Gao[3,7,8], Yi Zhang[1,2*]

Affiliations

[1] Department of Biomedical Engineering, University of Connecticut, Storrs, CT 06269, USA.

[2] Institute of Materials Science, University of Connecticut, Storrs, CT 06269, USA.

[3] Department of Chemical and Biomolecular Engineering, Rice University, Houston, TX 77005, USA.

[4] Department of Pathology and Laboratory Medicine, UConn Health, Farmington, CT 06030, USA

[5] Division of Infectious Diseases, Department of Medicine, UConn Health, Farmington, CT 06030, USA

[6] Department of Chemistry, University of Nebraska-Lincoln, Lincoln, NE 68588, USA.

[7] Department of Bioengineering, Rice University, Houston, TX 77005, USA.

[8] Department of Chemistry, Rice University, Houston, TX 77005, USA.

[#] Current address: Department of Biochemistry and Molecular Biology, School of Basic Medical Sciences, Tianjin Medical University, Tianjin, 300070 China.

[†] These authors contributed equally to this work.

* Corresponding author. Email: yi.5.zhang@uconn.edu (Y.Z.)

ABSTRACT

Rapid and ultrasensitive point-of-care RNA detection plays a critical role in the diagnosis and management of various infectious diseases. The gold-standard detection method of reverse transcription-quantitative polymerase chain reaction (RT-qPCR) is ultrasensitive and accurate yet limited by the lengthy turnaround time (1-2 days). On the other hand, antigen test offers rapid at-home detection (15-20 min) but suffers from low sensitivity and high false-negative rates. An ideal point-of-care diagnostic device would combine the merits of PCR-level sensitivity and rapid sample-to-result workflow comparable to antigen testing. However, the existing detection platform typically possesses superior sensitivity or rapid sample-to-result time, but not both. This paper reports a point-of-care microfluidic device that offers ultrasensitive yet rapid detection of viral RNA from clinical samples. The device consists of a microfluidic chip for precisely manipulating small volumes of samples, a miniaturized heater for viral lysis and ribonuclease (RNase) inactivation, a CRISPR Cas13a- electrochemical sensor for target preamplification-free and ultrasensitive RNA detection, and a smartphone-compatible potentiostat for data acquisition. As demonstrations, the devices achieve the detection of heat-inactivated SARS-CoV-2 samples with a limit of detection down to 10 aM within 25 minutes, which is comparable to the sensitivity of RT-PCR and rapidness of antigen test. The platform also successfully distinguishes all nine positive unprocessed clinical SARS-CoV-2 nasopharyngeal swab samples from four negative samples within 25 minutes of sample-to-result time. Together, this device provides a point-of-care solution that can be deployed in diverse settings beyond laboratory environments for rapid and accurate detection of RNA from clinical samples. The device can potentially be expandable to detect other viral targets, such as human immunodeficiency virus (HIV) self-testing and Zika virus, where rapid and ultrasensitive point-of-care detection is required.

INTRODUCTION

The rapid and ultrasensitive point-of-care nucleic acid testing from clinical samples plays critical roles in the diagnosis and management of infectious diseases, ranging from human papillomavirus infection to SARS-CoV-2 and human immunodeficiency virus (HIV) self-testing. As the predominant technique for nucleic acid testing [1], RT-qPCR relies on a series of lengthy steps from nucleic extraction to target amplification and readout acquisition, totaling over four hours. In addition, such a complicated, multi-step process often involves frequent manipulation of liquids and runs the risk of sample cross-contaminations, resulting in false-positive or false-negative test results. Finally, the essential thermocycling during amplification and the need for expensive optical instruments for fluorescence intensity measurement limit the availability of RT-qPCR primarily to laboratories. To date, a vast majority of point-of-care platforms for the diagnosis and management of infectious diseases rely on the rapid antigen (typically ~15 min) or antibody (typically less than 30 min) tests, which, however, suffer from low sensitivity (most rapid antigen tests) [2, 3], limited diagnostic values due to the delayed presence (days to weeks) of antibodies (antibody tests) [4, 5], or high false-negative rates [6-8]. An ideal point-of-care nucleic acid testing device should satisfy the requirements of both high sensitivities, preferably at the PCR level, and a short detection time comparable to antigen testing (typically ~15 min).

Recent endeavors in the understanding of CRISPR and CRISPR-associated (Cas) protein systems have presented new opportunities for nucleic acid detection [9-11] . The CRISPR-Cas system constitutes a significant prokaryotic adaptive immune system against viral infections [12-14]. CRISPR-Cas endonucleases, especially extensively researched Cas9, Cas12a, and Cas13a, demonstrate on-target cleavage when complexed with a guide RNA, thus effectively destroying invading nucleic acids via complementary base pairing [10, 15]. The sequence-based targeting

capability of the CRISPR-Cas system has inspired the development of CRISPR-based diagnostics [16, 17]. Among various CRISPR-Cas endonucleases, Cas13a receives much attention for nucleic acid testing due to its unique collateral cleavage activity; Upon target recognition, the catalytic domains of the protein are activated, which not only cleaves target RNA but also enables nonspecific and sequence-independent cleavage of nearby single-stranded RNA (ssRNA) labeled with fluorescent or colorimetric reporters in a manner [18, 19], resulting in the transducing of target-recognition into measurable sensor signals. Building on this collateral cleavage activity of Cas13a protein, various CRISPR Cas13a-based detection platforms, including SHERLOCK [20] and Cas13a-graphene field-effect transistors [21], have been developed for the highly specific and sensitive detection of viral RNA and other pathogenic RNA targets.

Recent studies also reported CRISPR Cas13a-based devices for point-of-care nucleic acid detections [22-28] . For example, Najjar et al. reported a point-of-care electrochemical device that extracts, concentrates, amplifies, and detects the SARS-CoV-2 from unprocessed saliva samples within 2 hours [29]. Nevertheless, the application of existing CRISPR-based devices in point-of-care nucleic acid testing still requires (1) complicated isothermal nucleic acid pre-amplifications (e.g., recombinase polymerase amplification, RPA or loop-mediated isothermal amplification, LAMP) [30, 31] or (2) lengthy and equipment-intensive RNA extraction and isolation steps. Therefore, there is an urgent need to develop a point-of-care device for nucleic acid testing without the need for complicated target amplification and lengthy RNA extraction and isolation steps.

Here, we report a point-of-care microfluidic device for rapid and ultrasensitive nucleic acid testing without the need for target preamplifications and lengthy nucleic extraction steps. The point-of-care device takes unprocessed clinical samples, inactivates ribonucleases and actively lyse viral RNAs by using integrated miniaturized Joule heaters, pneumatically pumps the lysed

viral samples into detection reservoirs, and performs the amplification-free nucleic acid detection using Cas13a-electrochemical sensors. As evidence of the detection capabilities, the device realizes a limit of detection (LOD) down to 10 aM with 25 min sample-to-result time by using heat-inactivated SARS-CoV-2 samples. Clinical validations using thirteen (nine positive and four negative) clinical SARS-CoV-2 nasopharyngeal swab samples further highlight the capability for accurate yet rapid RNA detection from unprocessed clinical samples. Most importantly, this device requires minimal operations, underlying the capability for point-of-care diagnostics.

RESULTS AND DISCUSSION

Design of a Point-of-Care Microfluidic Device for Rapid and Ultrasensitive RNA Detection

Nucleic acid detection in patient samples is often preceded by nucleic acid extraction from viral particles. However, since biological matrices such as nasopharyngeal swab specimens contain nucleases that can degrade crRNA[32], an essential CRISPR assay reagent for target recognition, the viral lysis and nuclease inactivation step should be separated from the detection reaction. For point-of-care applications, the sample volume is generally small, and therefore, the manipulation of liquids between these two steps is commonly assisted by microfluidics. In addition, thermochemical pretreatment has a long history in nucleic acid extraction and amplification-based detection [33-35]. Recently, this method has demonstrated its compatibility with CRISPR assay[36, 37]. As a result, a heating unit for the active lysis of viral particles is desired. A final consideration in the design of a point-of-care platform is the deployment of a user-friendly data acquisition system. For certain techniques, such as surface-enhanced Raman spectroscopy [38, 39], this requirement can be substantially challenging as it needs a high-power laser source and a sophisticated optical

sensing module. In contrast, electrochemical sensors based on commercially available screen-printed electrodes have been widely used in wearable electronics, implantable bioelectronics, and point-of-care applications [40, 41]. In particular, smartphones are excellent candidate in point-of-care settings, and electrochemical signal readout by smartphones has already been extensively investigated [42, 43].

Taking into account the above design principles, we designed a point-of-care device with four key components for rapid and ultrasensitive RNA detection from unprocessed clinical samples (**Figures 1A and B**): 1) a microfluidic chip consisting of a lysis reservoir, a detection reservoir, and microchannels, allowing precise manipulation of small volumes of samples and preventing sample evaporation and contamination; 2) a miniaturized and battery-powered Joule heater for thermochemical lysis of viral particles and ribonuclease (RNase) inactivation, thereby eliminating the need for traditional RNA extraction and purification steps; 3) a CRISPR Cas13a-based electrochemical biosensor for ultrasensitive and target preamplification-free detection of viral RNA; 4) a USB potentiostat for data acquisition and communication to a graphical user interface (GUI) on a smartphone. **Figure 1C** illustrates the overall operation of the device for viral RNA detection from unprocessed clinical samples. Specifically, a nasopharyngeal swab sample is first transferred into a lysis buffer and then injected into the lysis reservoir via a pipette or dropper. The microheater is then activated to actively lyse viral particles and inactivate RNases (95 ºC for 10 min). Following thermochemical treatment, the sample solution is pneumatically pumped into the detection reservoir by pushing air from the pipette or dropper. Viral RNA detection mediated by Cas13a collateral cleavage occurs in the detection reservoir, and electrochemical signals are recorded by the smartphone-controlled portable potentiostat.

Thermochemical Treatment for Minimally Instrumented and Efficient Viral RNA Extraction

Lysing viral particles to extract genetic material is an essential step in nucleic acid-based viral disease diagnostics. Conventional methods use proprietary reagents and silica-based columns to isolate viral RNAs from samples [44]; however, these extraction and purification steps are instrument-intensive and time-consuming. Recent studies have demonstrated that a combination of heating and chemical treatment can effectively lyse viral particles and inactivate RNases present in samples [45, 46]. This accelerated RNA extraction procedure is crucial to a fast detection workflow. To optimize the performance of SARS-CoV-2 RNA extraction, we evaluated the lysis efficiency of SARS-CoV-2 viral particles in a lysis buffer with six different heating durations (0, 5, 10, 15, and 30 min) at a lysis temperature of 95 °C. Here, the lysis efficiency is defined as the percentage of thermochemically extracted viral RNA copies, quantified by RT-qPCR, among a known viral load. The QuickExtract™ Solution was used as the lysis buffer since it does not interfere with the trans-cleavage efficiency of CRISPR assay [23]. For a total virus input of approximately 602 copies/μL, 88.4 % (532 copies/μL) of the inactive virus was lysed after heating for 5 min, and 10 min heating increased the lysis efficiency to 99 % (596 copies/μL) (**Figures 2A and B**). A heating duration of 15 min yielded the highest level of extracted RNAs, which is slightly higher than the total input copy number. This error may arise from random error and calibration error from RT-qPCR. Considering the sufficiently high lysis efficiency and preferably a fast process, we used 10 min as the lysis time in the following experiments.

Encouraged by these results, we employed a miniaturized Joule heater in the platform to streamline the thermochemical treatment for point-of-care applications. The microheater is composed of patterned traces of conductive materials in a serpentine geometry, and heat generation

is governed by Joule's law when an electric current passes through the resistive pattern. **Figure 2C** shows an optical image of a commercially available Joule microheater on a polyimide substrate and a set of infrared thermographic images of continuous heat generation over 10 min. The current supplied by a regular 1.5 V AAA battery was capable of raising the temperature to ~95 °C within 30 seconds and could maintain roughly the same temperature for at least 10 min. This demonstrates the capability of using a single AAA battery to operate the microheater for thermochemical lysis of virus. The battery can be used for two to three tests. Importantly, the heating was highly localized within the designated area as a result of the low thermal conductivity of polyimide (0.004 W/m·K), which minimizes heat dissipation and potential negative effects on CRISPR reagents (for example, denaturation of Cas13a) housed in the detection reservoir.

Cas13a-Mediated Electrochemical Detection of Viral RNA

In our recent study[47], we successfully enhanced the binding affinities of LwaCas13a to both target and reporter RNAs by fusing an RNA-binding domain, heterogeneous nuclear ribonucleoprotein A1 RNA-recognition motif 2 (RBD#3), to a unique β-hairpin loop proximal to the active site of LwaCas13a. The resultant Cas13a fusion protein exhibited dramatically increased collateral activity and achieved attomolar detection of SARS-CoV-2 N gene synthetic RNA fragments on conventional screen-printed electrodes without target preamplifications. Nevertheless, the reported Cas13a-electrochemical biosensor relies on the measurement of electron transfer in the Tris-HCl (10 mM) / NaCl (100 mM) buffer environment before and after the CRISPR reactions, which requires additional sample washing steps for the data acquisition. Such an operation protocol is not compatible with point-of-care applications.

Here, we developed a Cas13a-electrochemical biosensor that does not require the sample washing steps and, therefore, can be integrated into a point-of-care detection platform. More specifically, the gold working electrode of a commercially available screen-printed electrochemical device is first functionalized with 5' thiol-modified, 20-nt uracil-only (polyU_{20}) reporters with redox-active methylene blue (MB) tags at the 3' end (**Figure 3A**). The electron transfer from MB to the electrode surface generates a redox current that can be interrogated by square-wave voltammetry (SWV). In the presence of target RNA, the engineered LwaCas13a forms a ternary ribonucleoprotein complex with crRNA and SARS-CoV-2 target RNA, thereby initiating nonspecific collateral cleavage of polyU_{20} reporters on the electrode surface. The collateral cleavage of MB in the vicinity of the electrode surface results in reduced electron transfer kinetics, causing a decrease in the measured peak current at the redox potential of MB (**Figure 3B**). The change in the SWV peak current in the testing solution, which contains target RNA, crRNA, and engineered LwaCas13a, can be correlated with the viral load. The relative change in the peak current after 30 min assay incubation time indicates a LOD down to 10 aM by using SARS-CoV-2 synthetic targets (**Figure 3C**). This LOD is consistent with our previous results where additional assay washing steps are needed, showing the capability for ultrasensitive nucleic acid RNA detection in complex CRISPR reaction medium (proteins and crRNAs) without the need for assay washing steps. We also studied the selectivity of our engineered CRISPR Cas13a-based electrochemical biosensor by exposing the platform to synthetic targets of SARS-CoV-2, influenza virus (INV), and respiratory syncytial virus (RSV). Notably, the sensor signals from the non-target viral RNA sequences (RSV and INV A and B) were significantly lower than that from our SARS-CoV-2 targets despite these non-targets viral RNA being present in a concentration an order of

magnitude higher than that of the target SARS-CoV-2 (**Figure 3D**), demonstrating the high selectivity of our engineered CRISPR Cas13a-based electrochemical biosensors.

Lyophilization and Rehydration of CRISPR Assay

The assembly of the CRISPR assay requires technical expertise in order to avoid contamination or compromised assay performance. Hence, besides sample treatment, it is also crucial to eliminate the assay preparation step for end-users in point-of-care settings. Previous studies have demonstrated that lyophilization could be adopted to store CRISPR assays in a portable format and that rehydration had negligible effects on assay performance in terms of collateral activity [20, 48, 49]. However, the majority of these studies focused on freeze-drying reagents on a paper substrate for lateral flow readout. It remains unclear whether cellulose fibers in a paper substrate affect the rehydration of freeze-dried assay. On one hand, capillary wetting of the paper could possibly accelerate reagent dissolution; on the other hand, the assay components may be trapped in the interwoven network of cellulose fibers or their internal mesoporous structure, hampering the activation of Cas13a proteins and collateral cleavage on the sensor interface as a result of diffusion limitation.

Aiming to gain insights into assay rehydration, we lyophilized CRISPR assay components on three different substrates (filter paper, weighing paper, and a polydimethylsiloxane, PDMS, membrane). The reagents were rehydrated in 10 mM Tris buffer spiked with 1 fM synthetic SARS-CoV-2 RNA target on screen-printed electrodes (**Figure 4A**). The time-sequential, background-subtracted SWV curves for the three substrates after rehydration in spiked target solution exhibit a gradual decrease in the peak current over the course of 30 min due to the cleavage of MB from polyU_{20} reporters (**Figures 4B, D,** and **F**). The signal responses after 30 min reaction showed a 20.48 % change when the CRISPR assay was lyophilized on a PDMS membrane, significantly

higher than the changes of 12.97 % and 15.59 % with filter paper and weighing paper, respectively (**Figures 4C, E, and G**). This result implies the potential importance of substrate material and microstructure in the lyophilization and rehydration of CRISPR assay. Additionally, despite lower responses on paper-based substrates, freeze-dried CRISPR assay still retained decent collateral activity after rehydration. Altogether, lyophilization is a suitable approach for the preservation of CRISPR reagents. The difference between paper-based substrates and PDMS substrates may arise from microstructural differences. In particular, the paper substrate with a fibrous mesh structure diminishes the diffusion of the CRISPR assay to the sensor surface. By storing CRISPR reagents in the PDMS-based detection chamber, the CRISPR Cas13a assay permits viral diagnostics at the point of use without labor-intensive and contamination-prone assay preparation.

Device Validation Using Heat-Inactivated and Clinical SARS-CoV-2 Samples

After validating each individual component of the device, we assembled the device to evaluate the detection capability against viral samples. Briefly, the microfluidic device with pre-loaded lyophilized CRISPR assay is attached to the screen-print-electrode by using a double-sided adhesive, and then the microheater is fixed below the lysis reservoir by using the same adhesive. Finally, a battery box is connected to the Joule heater to finish the assembly of the device. As an initial demonstration, we spiked heat-inactivated SARS-CoV-2 (VR-1986HK™, ATCC Manassas, VA, USA) in 10 mM Tris buffer (pH 8.0) and then mixed the sample with QuickExtract™ lysis buffer at a 1:1 volumetric ratio. The final solution was injected into the assembled device, and the detection process followed the workflow as illustrated previously in **Figure 1C**. After the lysed sample was pumped into the detection chamber to rehydrate lyophilized CRISPR reagents, the time-sequential SWV curves were recorded at 10 s intervals for 30 min. The change in peak currents for the negative controls quickly plateaued, while the signal responses for heat-inactivated

SARS-CoV-2 at different concentrations had an initial steep rise followed by a steady increase at a much slower rate (**Figure 5A**). Notably, the changes at 10 min reaction time were sufficient to determine target concentration and yielded a LOD of 10 aM for heat-inactivated SARS-CoV-2 detection (**Figure 5B**), and therefore, is used for our following studies.

For clinical validation, a total of 13 nasopharyngeal samples were tested, including RT-qPCR confirmed four negative samples and nine positive samples. Our device successfully differentiated all negative clinical samples from all positive ones when the cutoff threshold (threshold=16.27 %) was defined as two standard deviations (σ=1.33 %) above the mean value (μ=13.61 %) of the signal responses (**Figure 5C and D**). Remarkably, the overall detection procedure from the injection of unprocessed samples to data collection took only 25 min to complete, including sample acquisition, thermochemical treatment, and CRISPR-electrochemical detection. Moreover, the operation required minimal effort, merely involving sample dilution, liquid injection, and manual pumping. In practical applications, all the chemicals (QuickExtract™ lysis buffer and Tris buffer) and tools (a dropper and a portable potentiostat) can be supplied along with the assembled point-of-care device, suggesting the potential for field deployment as a truly point-of-care diagnostic platform.

CONCLUSION

Despite numerous attempts, a considerable number of CRISPR-based biosensors have yet to truly bypass nucleic acid amplification while attaining a clinical level of detection limit (**Table 1**). On the other hand, field deployment of preamplification-free techniques is still facing substantial challenges, including significantly compromised sensitivity following integration into a point-of-care device and expensive instrumentation, especially for certain optical methods. To

tackle these problems, we developed an easy-to-use, sample-to-result electrochemical biosensing system with a smartphone readout. The microfluidic chip, pre-loaded with lyophilized CRISPR assay reagents and coupled with a battery-powered microheater, not only keeps samples free of cross-contamination, thereby improving diagnostic accuracy, but also establishes a streamlined workflow with minimal user operations for RNA extraction and nuclease inactivation from unprocessed clinical samples. Moreover, the enhanced collateral activity of engineered Cas13a allows for amplification-free detection with ultrahigh sensitivity within a short amount of time. Hence, our device realizes an ultralow LOD (10 aM) within 25 min, comparable to one of the most sensitive CRISPR-based nucleic acid detection platforms, Cas13a graphene field-effect transistors [21]. To our knowledge, this is among the most sensitive CRISPR-based point-of-care detection platform reported thus far. Such high sensitivity achieved by conventional screen-printed electrodes greatly facilitates broad distribution to end-users as the large-scale manufacturing process does not involve complex and expensive cleanroom-based micro/nanofabrication techniques often required by other ultrasensitive CRISPR-based amplification-free biosensors [21, 50]. The point-of-care application of the device also benefits from the wide availability of other device components. For example, the preparation of microfluidic chip is compatible with 3D printing of molds and subsequent PDMS casting for mass production, and the portable potentiostat for user-friendly data acquisition via smartphone is commercially available.

Overall, we have demonstrated a point-of-care platform for ultrasensitive SARS-CoV-2 detection within 25 minutes of sample-to-results time from patient samples. The cost of the disposable module comprising the microfluidic chip, CRISPR assay, microheater, and screen-printed electrodes is estimated to be ~$15 (**Table S1**). Future work will aim to 1) further validate the device performance beyond SARS-CoV-2 detection, 2) study the assay storage ability, and 3)

adapt the device design for targeting DNA samples by simply replacing the Cas 13a with Cas 12a and associated reporters.

MATERIALS AND METHODS

Functionalization of Screen-Printed Electrodes

The screen-printed electrode C223BT (Metrohm, Herisau, Switzerland) is a three-electrode system in which the working and counter electrodes are made of gold and the reference electrode is made of silver. Here, we functionalized polyU_{20} reporter tagged with redox-active methylene blue (**Table S2**; Integrated DNA Technologies, IA, USA) on the working electrode via thiol-gold chemistry. The surface functionalization follows the protocol developed in our recent study[47]. Briefly, the More specifically, we first mixed 2 μL of 200 μM tris(2-carboxyethyl) phosphine (>98%; Sigma-Aldrich, MO, USA) with 2 μL of 100 μM polyU_{20}-MB reporter to reduce the disulfide bond at room temperature for 10 min. We then brought the reporter concentration down to 8.33 μM by adding 20 μL of 10 mM Tris hydrochloride buffer (Tris-HCl, pH 8.0; Fisher Bioreagents, PA, USA). A 6 μL droplet of the reporter solution was added to the working electrode, followed by incubation at room temperature for 2 h. Subsequently, the functionalized electrode was rinsed with nuclease-free water and passivated by incubating the electrode in 6 μL of 2 mM 6-mercapto-1-hexanol (>98%; TCI America, OR, USA) for 1 h to prevent nonspecific adsorption and ensure upright reporter orientation on the surface. Finally, after thoroughly rinsed with water, the electrode was incubated in 10 mM Tris-HCl buffer at 40 °C for 10 min to remove weakly bound reporters.

Engineered Cas13a Protein Purification

The engineered LwaCas13a protein was produced as described previously[47]. Briefly, the transformed *E. coli* BL21(DE3) cells were grown overnight on an LB agar with ampicillin selection. Single colonies were inoculated and induced with IPTG. 16 hours after induction, cells were harvested and lysed by sonication and purified by Ni-NTA affinity chromatography. The His-SUMO fusion tag was cleaved by SUMO protease. Purified protein was stored at -80 °C until use.

Target RNA Preparation

The target RNA was obtained by in vitro transcription (IVT) as previously described [47]. Briefly, the HiScribe T7 Quick High Yield RNA Synthesis kit (New England Biolabs) was used per the manufacturer's instructions, with 0.5 μM of gBlock (Integrated DNA Technologies) containing a T7 promoter sequence as the IVT template. The reactions were incubated at 37 °C for 4 h and purified with RNAClean XP beads (Beckman Coulter) after DNase I treatment. RNAs were stored at -80 °C before use.

Fabrication of Microfluidic Devices

The fabrication of microfluidic devices started with 3D printing (Form 2; Formlabs, MA, USA) to produce a mold (Clear Resin V4; Formlabs, MA, USA) with a set of microfluidic channels (cross-sectional width: 0.5 mm, height: 0.5 mm), a viral lysis reservoir (diameter: 7 mm, height: 0.5 mm), and a detection reservoir (diameter: 7 mm, height: 1 mm) (**Figure S1**). Polydimethylsiloxane (PDMS, SYLGARD™ 184 Silicone Elastomer Kit, 10:1 weight ratio of elastomer/curing agent; Dow Corning, MI, USA) was degassed in a vacuum desiccator, cast into the mold, and cured in an oven at 65 ºC for 2 h to form a 3-mm-thick microfluidic channel layer. Spin-casting PDMS (10:1 w/w mixture of elastomer and curing agent) on a glass slide at 1000 rpm

for 60 s (WS-650Mz-23NPPB; Laurell Technologies, PA, USA) and then curing at 65 °C for 2 h yielded a 50-µm-thick bottom layer. A mechanical punch (Integra™ 3337, diameter: 8 mm; Integra, NJ, USA) created a hole on the bottom layer to allow the reaction between the assay in the detection reservoir and the reporters on the surface of the working electrode. The two PDMS layers were bonded by corona treatment (BD-20; Electro-Technic Products, IL, USA) for 5 min and left at room temperature overnight.

Device Assembly

The point-of-care device consists of four components: a microfluidic device, a reporter-functionalized screen-printed electrode, a heating unit, and a power supply unit. The device assembly started with using a double-sided adhesive (Medical Tape 1509; 3M, MN, USA) to bond the microfluidic device and the screen-printed electrode, by which the detection reservoir was aligned with the working electrode modified with polyU_{20}-MB reporters. A miniaturized Joule heater was then attached underneath the viral lysis reservoir. Finally, a regular 1.5 V AAA battery was connected to the Joule heater to provide power.

Characterization of Thermochemical Treatment for RNA Extraction

For the evaluation of lysis efficiency, heat-inactivated SARS-CoV-2 (VR-1986HK™, ATCC Manassas, VA, USA) with a viral load of 3.9×10^5 copies/µL was diluted in 10 mM Tris-HCl buffer into a final concentration of ~602 copies/µL. The viral sample was mixed with QuickExtract™ Extraction Solution (Lucigen, Middleton, WI, USA) at a 1:1 volumetric ratio and incubated at 95 °C in a digital dry bath (Thermo Scientific, MA, USA) for various periods of time (0, 5, 10, 15, and 30 min). The concentration of extracted RNA was quantified by RT-qPCR and

used to calculate the lysis efficiency, defined as the percentage of RNA extracted from a sample with a known viral load.

For the characterization of continuous heat generation, a 1.5 V AAA battery was connected to a microheater to initiate heating, and an infrared camera (E6-XT; FLIR, OR, USA) captured thermographic images at different times of the heating process (30 s, 1 min, 5 min, and 10 min) to measure temperature.

Detection of SARS-CoV-2 Synthetic RNA Targets

The sequence information of crRNA and synthetic SARS-CoV-2 N gene fragment can be found in **Table S2**. A 40 μL CRISPR assay was prepared, containing 50 mM Tris-HCl buffer, 5 mM $MgCl_2$ (Invitrogen, MA, USA), 45 nM engineered LwaCas13a which was expressed and purified as previous study [47], 1 U/μL murine RNase inhibitor (New England Biolabs, MA, USA), 22.5 nM crRNA (Sangon Biotech, Shanghai, China), and various concentrations of SARS-CoV-2 RNA target. 40 μL assembled CRISPR assay was added to the microfluidic chip and pumped to the reporter functionalized working electrode of the screen-printed electrode. A portable potentiostat (Sensit Smart; PalmSens, Netherlands) was used to collect the SWV. Then, the CRISPR assay was applied to the electrodes and allowed to incubate for 30 min. During the cleavage, SWV curve was recorded for each 10 second.

Lyophilization of CRISPR Reagents

For lyophilization of CRISPR assay components, a 4.6 μL solution containing 5 mM $MgCl_2$, 50 mM Tris-HCl buffer, 22.5 nM crRNA, and 45 nM engineered LwaCas13a was added to three different substrates (filter paper, weighing paper, and a PDMS membrane). Then, the CRISPR reagents were lyophilized at -50 °C under a vacuum of 0.005 mTorr for 4 h (FreeZone

4.5 Liter -84C Benchtop Freeze Dryers, Labconco, MO, USA) after initial freezing at -80 °C for 1 h. To load into the device, the reagent solution was injected into the detection reservoir through the inlet port and then lyophilized. The microfluidic chip was transferred to a sealed Petri dish for storage in a -80 °C freezer.

Evaluation of Rehydrated CRISPR Assay Performance

The CRISPR assay was initially loaded onto a substrate membrane, which was then subjected to lyophilization. Next, the lyophilized substrate was carefully placed face-down onto the screen-printed working electrode. To prevent any potential evaporation effects, a microfluidic chip was utilized to cover the working electrode. SARS-CoV-2 N gene RNA fragments were spiked into the droplet to a final concentration of 1 fM and pumped to detection reservoir. Finally, the time-sequential SWV curves were measured by a portable potentiostat over 30 min after the rehydration process started.

Validation of Device for SARS-CoV-2 Detection in Heat-Inactivated Viral and Clinical Samples

Heat-inactivated SARS-CoV-2 was first diluted with 10 mM Tris-HCl buffer followed by adding an equal volume of QuickExtract™ lysis buffer. Next, 40 μL target solution was pipetted into the device, and the integrated heating element was activated to extract viral RNA in the lysis reservoir. To activate heating element, we use test hooks clips (080014-ND, Digi-Key, MN, USA) to connect battery box with heating element. After 10 min lysis, we disconnect the connection between battery box and heating element. The sample was cooled from 95 °C down to room temperature within 3 minutes (**Figure S2**). Then, 20 μL air was pipetted into the device to pneumatically pump the sample into the detection reservoir, where rehydration of lyophilized

CRISPR reagents occurred. SWV measurement by a portable potentiostat started immediately after the sample flowed into the detection reservoir. The signals were recorded over 30 min.

Clinical samples of nasopharyngeal swabs in viral transport medium (VTM) were obtained from UConn Health hospital or UConn Drive Through COVID Testing Center. Before transferring the samples to Dr. Zhang's lab at the University of Connecticut, both positive and negative samples were inactivated at 60 °C for 30 min. This research obtains ethical approval from the UConn Health Institutional Review Board.

For SARS-CoV-2 RNA detection from unprocessed clinical samples, 1 μL clinical sample was mixed with 1 μL of QuickExtract™ buffer, followed by a 20-fold dilution by adding 38 μL 10mM Tris-HCl buffer. The sample underwent the same detection procedure as the heat-inactivated virus.

Electrochemical Analysis

We used SWV to measure the electron transfer between the working electrode and redox-active polyU_{20}-MB reporters functionalized on the screen-printed electrode. For SARS-CoV-2 detection in synthetic SARS-CoV-2 targets, heat-inactivated and clinical samples, time-sequential SWV is performed every 10 s till the termination of the detection; the scan window was set to be -0.38 V to -0.04 V at 50 Hz using a portable potentiostat (Sensit Smart), and the software PSTrace high-level smoothing was used to eliminate signal noise. The background-subtracted peak electrochemical current change is given below:

$$\Delta I = \frac{I_0 - I}{I_0} \quad (1)$$

where I_0 and I are background-subtracted peak electrochemical current before and after the reaction, respectively. In this study, the LOD is defined as the lowest SARS-CoV-2 target concentration which gives a sensor signal significantly higher than that of the blank sample, with a confidence level of 95%.

ACKNOWLEDGEMENTS

We acknowledge the funding support by the University of Connecticut start-up fund (to Y.Z.), NSF CBET-2103025 and ECCS-2113736 (to Y.Z.), Rice University Startup fund (to X.G.), and NSF CBET-2031242 (to X.G.).

CONFLICT OF INTEREST

The authors declare no conflict of interest.

STATISTICS

Experimental data are expressed as the mean ± standard deviation (SD). Two-tailed P values were calculated using unpaired t-tests with Welch's correction. The software used for statistical analysis is OriginPro 2022.

ADDITIONAL INFORMATION

Supplementary Information

DATA AND MATERIALS AVAILABILITY: All data needed to evaluate the conclusions in the paper are present in the paper and/or the Supplementary Information.

REFERENCES

1. B. D. Kevadiya, J. Machhi, J. Herskovitz, M. D. Oleynikov, W. R. Blomberg, N. Bajwa, D. Soni, S. Das, M. Hasan, M. Patel, A. M. Senan, S. Gorantla, J. McMillan, B. Edagwa,

R. Eisenberg, C. B. Gurumurthy, S. P. M. Reid, C. Punyadeera, L. Chang and H. E. Gendelman, *Nat Mater*, 2021, **20**, 593-605.

2. *World Health Organization*, 2020, **https://www.who.int/news-room/commentaries/detail/advice-on-the-use-of-point-of-care-immunodiagnostic-tests-for-covid-19**.
3. M. Dohla, C. Boesecke, B. Schulte, C. Diegmann, E. Sib, E. Richter, M. Eschbach-Bludau, S. Aldabbagh, B. Marx, A. M. Eis-Hubinger, R. M. Schmithausen and H. Streeck, *Public Health*, 2020, **182**, 170-172.
4. B. Udugama, P. Kadhiresan, H. N. Kozlowski, A. Malekjahani, M. Osborne, V. Y. C. Li, H. Chen, S. Mubareka, J. B. Gubbay and W. C. W. Chan, *ACS Nano*, 2020, **14**, 3822-3835.
5. Q. X. Long, B. Z. Liu, H. J. Deng, G. C. Wu, K. Deng, Y. K. Chen, P. Liao, J. F. Qiu, Y. Lin, X. F. Cai, D. Q. Wang, Y. Hu, J. H. Ren, N. Tang, Y. Y. Xu, L. H. Yu, Z. Mo, F. Gong, X. L. Zhang, W. G. Tian, L. Hu, X. X. Zhang, J. L. Xiang, H. X. Du, H. W. Liu, C. H. Lang, X. H. Luo, S. B. Wu, X. P. Cui, Z. Zhou, M. M. Zhu, J. Wang, C. J. Xue, X. F. Li, L. Wang, Z. J. Li, K. Wang, C. C. Niu, Q. J. Yang, X. J. Tang, Y. Zhang, X. M. Liu, J. J. Li, D. C. Zhang, F. Zhang, P. Liu, J. Yuan, Q. Li, J. L. Hu, J. Chen and A. L. Huang, *Nat Med*, 2020, **26**, 845-848.
6. A. Harrington, B. Cox, J. Snowdon, J. Bakst, E. Ley, P. Grajales, J. Maggiore and S. Kahn, *J Clin Microbiol*, 2020, **58**.
7. M. C. Smithgall, I. Scherberkova, S. Whittier and D. A. Green, *J Clin Virol*, 2020, **128**, 104428.
8. C. A. Hogan, M. K. Sahoo, C. Huang, N. Garamani, B. Stevens, J. Zehnder and B. A. Pinsky, *J Clin Virol*, 2020, **128**, 104410.
9. G. J. Knott and J. A. Doudna, *Science*, 2018, **361**, 866-869.
10. A. Pickar-Oliver and C. A. Gersbach, *Nat Rev Mol Cell Biol*, 2019, **20**, 490-507.
11. M. Adli, *Nat Commun*, 2018, **9**, 1911.
12. F. J. Mojica, G. Juez and F. Rodriguez-Valera, *Mol Microbiol*, 1993, **9**, 613-621.
13. Y. Ishino, M. Krupovic and P. Forterre, *J Bacteriol*, 2018, **200**.
14. Y. Ishino, H. Shinagawa, K. Makino, M. Amemura and A. Nakata, *J Bacteriol*, 1987, **169**, 5429-5433.
15. K. S. Makarova, Y. I. Wolf, J. Iranzo, S. A. Shmakov, O. S. Alkhnbashi, S. J. J. Brouns, E. Charpentier, D. Cheng, D. H. Haft, P. Horvath, S. Moineau, F. J. M. Mojica, D. Scott, S. A. Shah, V. Siksnys, M. P. Terns, C. Venclovas, M. F. White, A. F. Yakunin, W. Yan, F. Zhang, R. A. Garrett, R. Backofen, J. van der Oost, R. Barrangou and E. V. Koonin, *Nat Rev Microbiol*, 2020, **18**, 67-83.
16. Z. Weng, Z. You, J. Yang, N. Mohammad, M. Lin, Q. Wei, X. Gao and Y. Zhang, *Angewandte Chemie International Edition*, 2023.
17. O. O. Abudayyeh, J. S. Gootenberg, S. Konermann, J. Joung, I. M. Slaymaker, D. B. Cox, S. Shmakov, K. S. Makarova, E. Semenova, L. Minakhin, K. Severinov, A. Regev, E. S. Lander, E. V. Koonin and F. Zhang, *Science*, 2016, **353**, aaf5573.
18. J. S. Gootenberg, O. O. Abudayyeh, J. W. Lee, P. Essletzbichler, A. J. Dy, J. Joung, V. Verdine, N. Donghia, N. M. Daringer, C. A. Freije, C. Myhrvold, R. P. Bhattacharyya, J. Livny, A. Regev, E. V. Koonin, D. T. Hung, P. C. Sabeti, J. J. Collins and F. Zhang, *Science*, 2017, **356**, 438-+.
19. J. S. Gootenberg, O. O. Abudayyeh, M. J. Kellner, J. Joung, J. J. Collins and F. Zhang, *Science*, 2018, **360**, 439-+.

20. J. S. Gootenberg, O. O. Abudayyeh, J. W. Lee, P. Essletzbichler, A. J. Dy, J. Joung, V. Verdine, N. Donghia, N. M. Daringer, C. A. Freije, C. Myhrvold, R. P. Bhattacharyya, J. Livny, A. Regev, E. V. Koonin, D. T. Hung, P. C. Sabeti, J. J. Collins and F. Zhang, *Science*, 2017, **356**, 438-442.
21. H. Li, J. Yang, G. Wu, Z. Weng, Y. Song, Y. Zhang, J. A. Vanegas, L. Avery, Z. Gao, H. Sun, Y. Chen, K. D. Dieckhaus, X. Gao and Y. Zhang, *Angewandte Chemie International Edition*, 2022, **61**.
22. M. M. Kaminski, O. O. Abudayyeh, J. S. Gootenberg, F. Zhang and J. J. Collins, *Nat Biomed Eng*, 2021, **5**, 643-656.
23. Y. Li, S. Li, J. Wang and G. Liu, *Trends Biotechnol*, 2019, **37**, 730-743.
24. R. Bruch, G. A. Urban and C. Dincer, *Trends Biotechnol*, 2019, **37**, 791-792.
25. M. Liang, Z. Li, W. Wang, J. Liu, L. Liu, G. Zhu, L. Karthik, M. Wang, K. F. Wang, Z. Wang, J. Yu, Y. Shuai, J. Yu, L. Zhang, Z. Yang, C. Li, Q. Zhang, T. Shi, L. Zhou, F. Xie, H. Dai, X. Liu, J. Zhang, G. Liu, Y. Zhuo, B. Zhang, C. Liu, S. Li, X. Xia, Y. Tong, Y. Liu, G. Alterovitz, G. Y. Tan and L. X. Zhang, *Nat Commun*, 2019, **10**, 3672.
26. R. Aman, A. Mahas and M. Mahfouz, *ACS Synth Biol*, 2020, **9**, 1226-1233.
27. M. Bao, Q. Chen, Z. Xu, E. C. Jensen, C. Liu, J. T. Waitkus, X. Yuan, Q. He, P. Qin and K. Du, *ACS Sens*, 2021, DOI: 10.1021/acssensors.1c00530.
28. R. A. Lee, H. Puig, P. Q. Nguyen, N. M. Angenent-Mari, N. M. Donghia, J. P. McGee, J. D. Dvorin, C. M. Klapperich, N. R. Pollock and J. J. Collins, *Proc Natl Acad Sci U S A*, 2020, **117**, 25722-25731.
29. D. Najjar, J. Rainbow, S. Sharma Timilsina, P. Jolly, H. De Puig, M. Yafia, N. Durr, H. Sallum, G. Alter and J. Z. Li, *Nature biomedical engineering*, 2022, **6**, 968-978.
30. A. Binnie, E. Fernandes, H. Almeida-Lousada, R. A. de Mello and P. Castelo-Branco, *Infection*, 2021, **49**, 377-385.
31. R. Nouri, Y. Jiang, X. L. Lian and W. Guan, *ACS Sens*, 2020, **5**, 1273-1280.
32. A. Wozniak, A. Cerda, C. Ibarra-Henriquez, V. Sebastian, G. Armijo, L. Lamig, C. Miranda, M. Lagos, S. Solari and A. M. Guzmán, *Scientific Reports*, 2020, **10**, 1-8.
33. Y. Liu, H. Ye, H. Huynh, C. Xie, P. Kang, J. S. Kahn and Z. Qin, *Nature communications*, 2022, **13**, 1687.
34. M. Karlikow, S. J. R. da Silva, Y. Guo, S. Cicek, L. Krokovsky, P. Homme, Y. Xiong, T. Xu, M.-A. Calderón-Peláez and S. Camacho-Ortega, *Nature Biomedical Engineering*, 2022, **6**, 246-256.
35. T. Zhang, R. Deng, Y. Wang, C. Wu, K. Zhang, C. Wang, N. Gong, R. Ledesma-Amaro, X. Teng and C. Yang, *Nature Biomedical Engineering*, 2022, **6**, 957-967.
36. S. S. Chandrasekaran, S. Agrawal, A. Fanton, A. R. Jangid, B. Charrez, A. M. Escajeda, S. Son, R. McIntosh, H. Tran, A. Bhuiya, M. D. De León Derby, N. A. Switz, M. Armstrong, A. R. Harris, N. Prywes, M. Lukarska, S. B. Biering, D. C. J. Smock, A. Mok, G. J. Knott, Q. Dang, E. Van Dis, E. Dugan, S. Kim, T. Y. Liu, J. R. Hamilton, E. Lin-Shiao, E. C. Stahl, C. A. Tsuchida, P. Giannikopoulos, M. McElroy, S. McDevitt, A. Zur, I. Sylvain, A. Ciling, M. Zhu, C. Williams, A. Baldwin, E. A. Moehle, K. Kogut, B. Eskenazi, E. Harris, S. A. Stanley, L. F. Lareau, M. X. Tan, D. A. Fletcher, J. A. Doudna, D. F. Savage and P. D. Hsu, *Nature Biomedical Engineering*, 2022, **6**, 944-956.
37. L. T. Nguyen, S. R. Rananaware, B. L. Pizzano, B. T. Stone and P. K. Jain, *Communications Medicine*, 2022, **2**, 7.

38. T. D. Payne, S. J. Klawa, T. Jian, S. H. Kim, M. J. Papanikolas, R. Freeman and Z. D. Schultz, *ACS sensors*, 2021, **6**, 3436-3444.
39. J.-H. Choi, M. Shin, L. Yang, B. Conley, J. Yoon, S.-N. Lee, K.-B. Lee and J.-W. Choi, *Acs Nano*, 2021, **15**, 13475-13485.
40. M. Wang, Y. Yang, J. Min, Y. Song, J. Tu, D. Mukasa, C. Ye, C. Xu, N. Heflin and J. S. McCune, *Nature Biomedical Engineering*, 2022, 1-11.
41. W. Tian, Y. Li, J. Zhou, T. Wang, R. Zhang, J. Cao, M. Luo, N. Li, N. Zhang and H. Gong, *ACS Applied Materials & Interfaces*, 2021, **13**, 8285-8293.
42. A. Ainla, M. P. Mousavi, M.-N. Tsaloglou, J. Redston, J. G. Bell, M. T. Fernández-Abedul and G. M. Whitesides, *Analytical chemistry*, 2018, **90**, 6240-6246.
43. A. C. Sun and D. A. Hall, *Electroanalysis*, 2019, **31**, 2-16.
44. N. Barak, R. Ben-Ami, T. Sido, A. Perri, A. Shtoyer, M. Rivkin, T. Licht, A. Peretz, J. Magenheim and I. Fogel, *Science Translational Medicine*, 2021, **13**, eabf2823.
45. C. Myhrvold, C. A. Freije, J. S. Gootenberg, O. O. Abudayyeh, H. C. Metsky, A. F. Durbin, M. J. Kellner, A. L. Tan, L. M. Paul, L. A. Parham, K. F. Garcia, K. G. Barnes, B. Chak, A. Mondini, M. L. Nogueira, S. Isern, S. F. Michael, I. Lorenzana, N. L. Yozwiak, B. L. MacInnis, I. Bosch, L. Gehrke, F. Zhang and P. C. Sabeti, *Science*, 2018, **360**, 444-448.
46. B. Ning, T. Yu, S. Zhang, Z. Huang, D. Tian, Z. Lin, A. Niu, N. Golden, K. Hensley, B. Threeton, C. J. Lyon, X. M. Yin, C. J. Roy, N. S. Saba, J. Rappaport, Q. Wei and T. Y. Hu, *Sci Adv*, 2021, **7**.
47. J. Yang, Y. Song, X. Deng, J. A. Vanegas, Z. You, Y. Zhang, Z. Weng, L. Avery, K. D. Dieckhaus and A. Peddi, *Nature Chemical Biology*, 2023, **19**, 45-54.
48. K. Pardee, A. A. Green, M. K. Takahashi, D. Braff, G. Lambert, J. W. Lee, T. Ferrante, D. Ma, N. Donghia, M. Fan, N. M. Daringer, I. Bosch, D. M. Dudley, D. H. O'Connor, L. Gehrke and J. J. Collins, *Cell*, 2016, **165**, 1255-1266.
49. P. Q. Nguyen, L. R. Soenksen, N. M. Donghia, N. M. Angenent-Mari, H. de Puig, A. Huang, R. Lee, S. Slomovic, T. Galbersanini, G. Lansberry, H. M. Sallum, E. M. Zhao, J. B. Niemi and J. J. Collins, *Nat Biotechnol*, 2021, DOI: 10.1038/s41587-021-00950-3.
50. J. Liang, P. Teng, W. Xiao, G. He, Q. Song, Y. Zhang, B. Peng, G. Li, L. Hu and D. Cao, *Journal of Nanobiotechnology*, 2021, **19**, 1-9.
51. R. Hajian, S. Balderston, T. Tran, T. Deboer, J. Etienne, M. Sandhu, N. A. Wauford, J.-Y. Chung, J. Nokes, M. Athaiya, J. Paredes, R. Peytavi, B. Goldsmith, N. Murthy, I. M. Conboy and K. Aran, *Nature Biomedical Engineering*, 2019, **3**, 427-437.
52. P. Fozouni, S. Son, M. Diaz de Leon Derby, G. J. Knott, C. N. Gray, M. V. D'Ambrosio, C. Zhao, N. A. Switz, G. R. Kumar, S. I. Stephens, D. Boehm, C. L. Tsou, J. Shu, A. Bhuiya, M. Armstrong, A. R. Harris, P. Y. Chen, J. M. Osterloh, A. Meyer-Franke, B. Joehnk, K. Walcott, A. Sil, C. Langelier, K. S. Pollard, E. D. Crawford, A. S. Puschnik, M. Phelps, A. Kistler, J. L. DeRisi, J. A. Doudna, D. A. Fletcher and M. Ott, *Cell*, 2021, **184**, 323-333 e329.
53. J. Joung, A. Ladha, M. Saito, M. Segel, R. Bruneau, M. W. Huang, N. G. Kim, X. Yu, J. Li, B. D. Walker, A. L. Greninger, K. R. Jerome, J. S. Gootenberg, O. O. Abudayyeh and F. Zhang, *medRxiv*, 2020, DOI: 10.1101/2020.05.04.20091231.

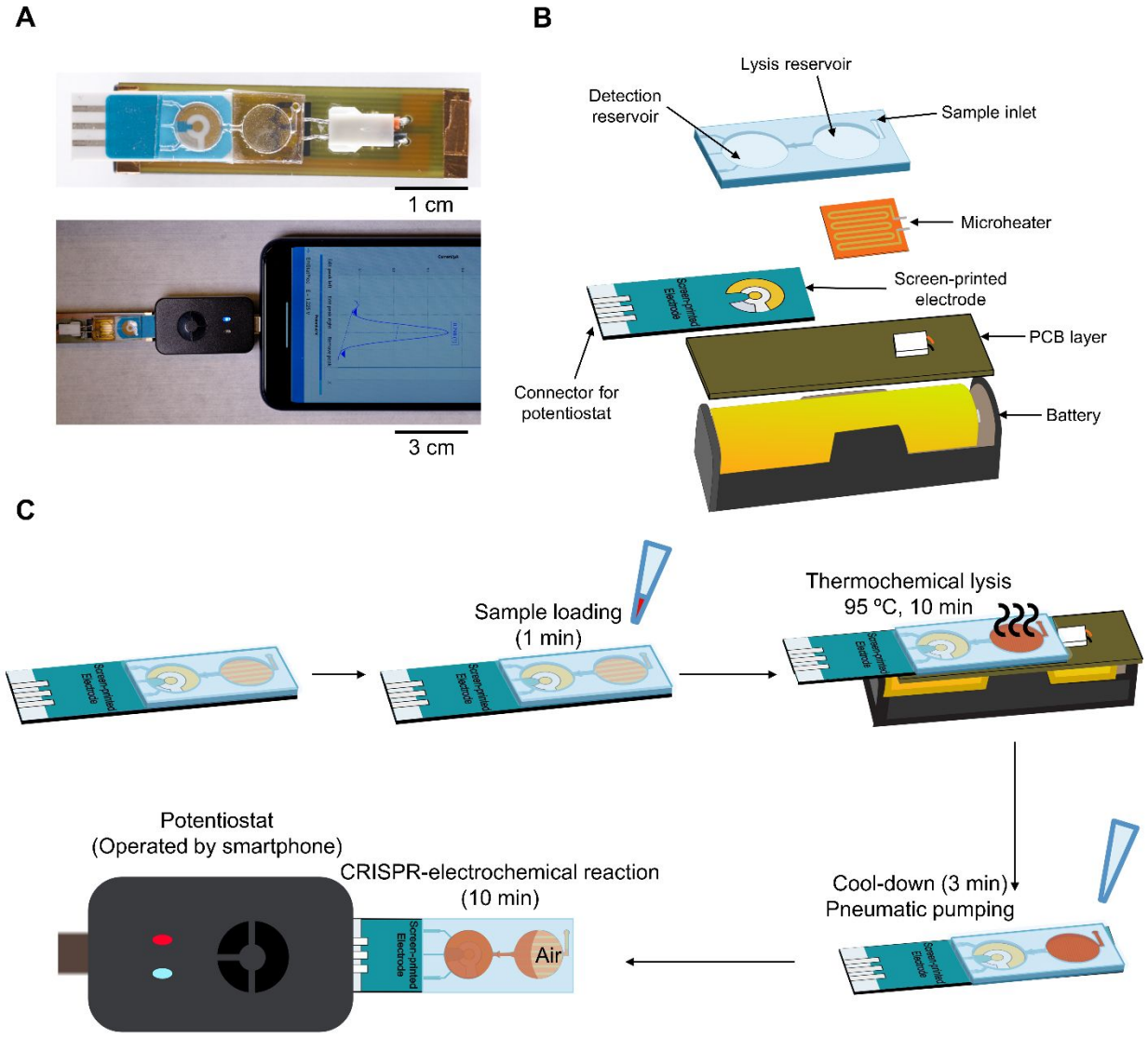

Figure 1. Overall design of the point-of-care device for rapid and ultrasensitive nucleic acid detection from unprocessed clinical samples. (A) Optical images of the device without the battery part (top) and a smartphone potentiostat readout system (bottom). (B) Exploded schematic illustration of the device, including microfluidic channels and reservoirs to guide sample flow and to create a sealed detection environment, a microheater for thermochemical treatment, a Cas13a-

electrochemical sensor, and a power supply part. (C) Workflow of viral detection from unprocessed patient samples. The sample-to-result time is ~25 min.

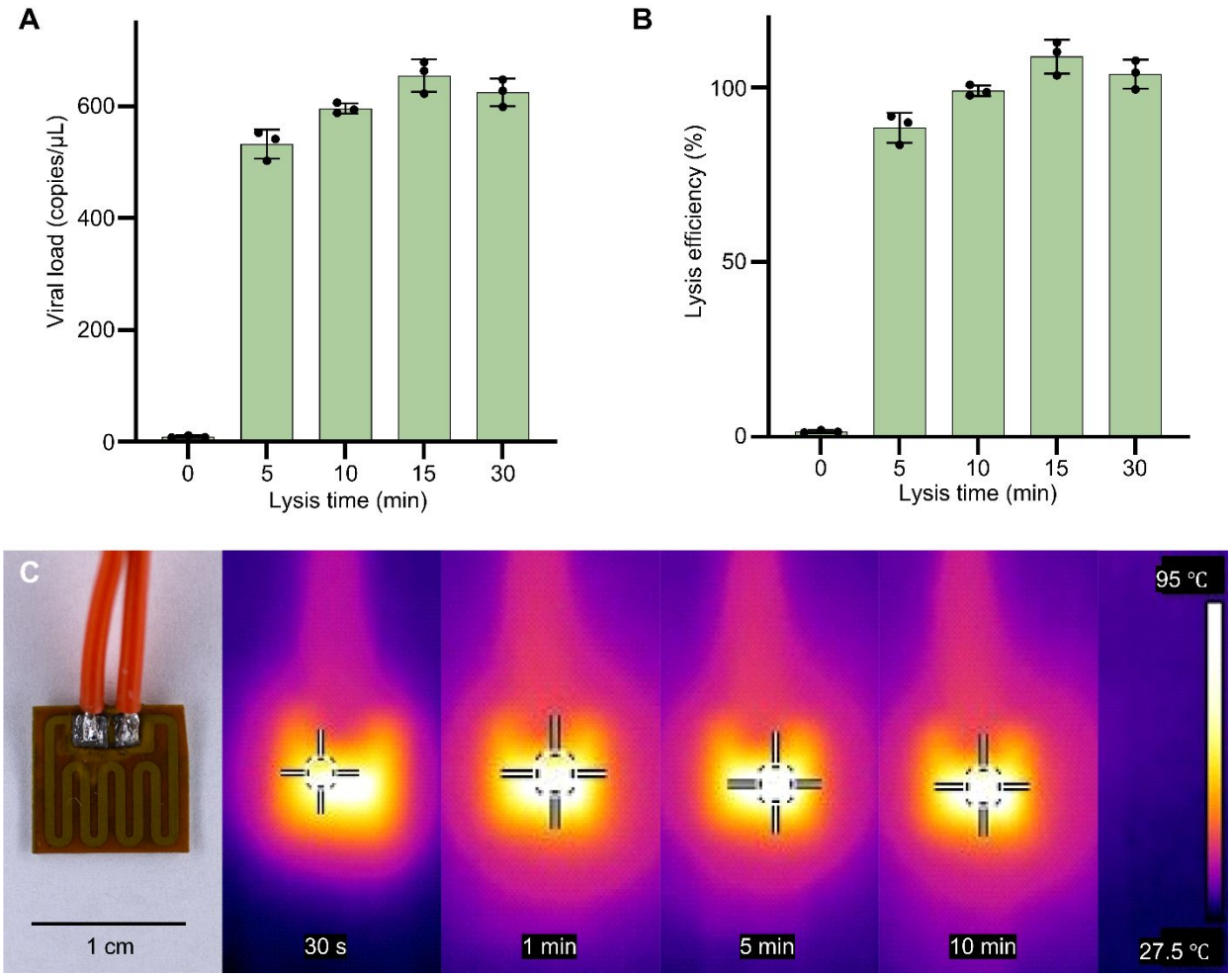

Figure 2. Characterization of viral lysis by using thermochemical treatment. (A) Extracted viral RNA load under different lysis durations. (B) Viral lysis efficiency with different lysis durations, calculated by dividing results in Figure 2A by the input heat inactivated virus load (602 copies/μL). (C) Infrared thermographic images for continuous operation of the microheater for 10 minutes.

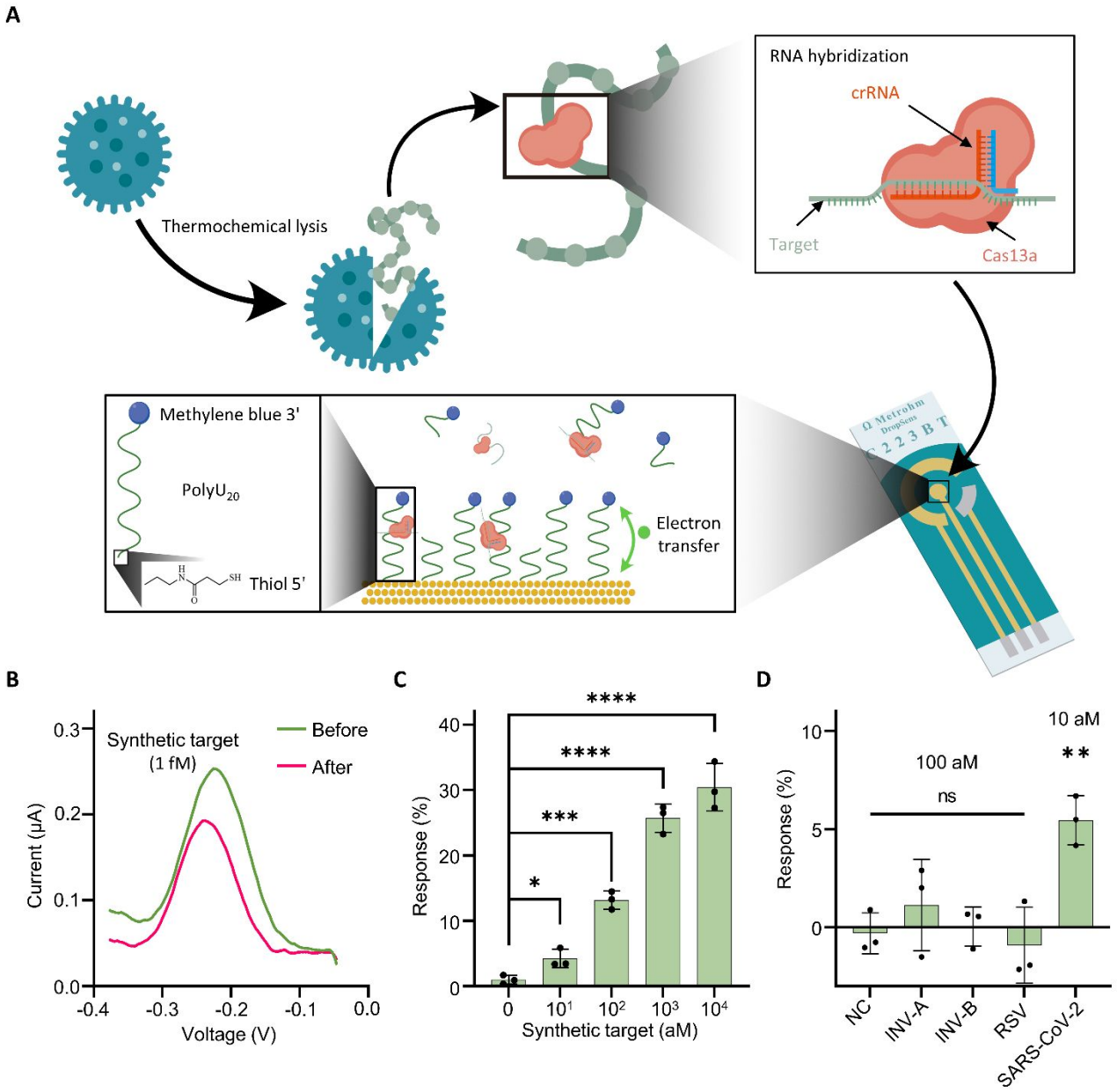

Figure 3. Validation of Cas13a-mediated electrochemical detection of SARS-CoV-2. (A) The working principle of Cas13a-mediated electrochemical detection of SARS-CoV-2. Target-specific activation of the engineered Cas13a by SARS-CoV-2 leads to the collateral cleavage of MB-tagged polyU$_{20}$ reporters on the screen-printed electrodes, resulting a decrease in electron transfer rate and a measurable peak current reduction. (B) A representation of SWV peak current change after the collateral cleavage of reporters. (C) Relative signal changes after 30 min of detection time at

different concentrations of SARS-CoV-2 synthetic targets (n = 3; *, $P < 0.05$; **, $P < 0.01$; ***, $P < 0.001$; ****, $P < 0.0001$). (D) Relative signal changes after 30 min of reaction with SARS-Cov-2 target and non-target viral RNA sequences (RSV and INV A and B) . (n = 3; ns: no significance; **, $P < 0.01$)

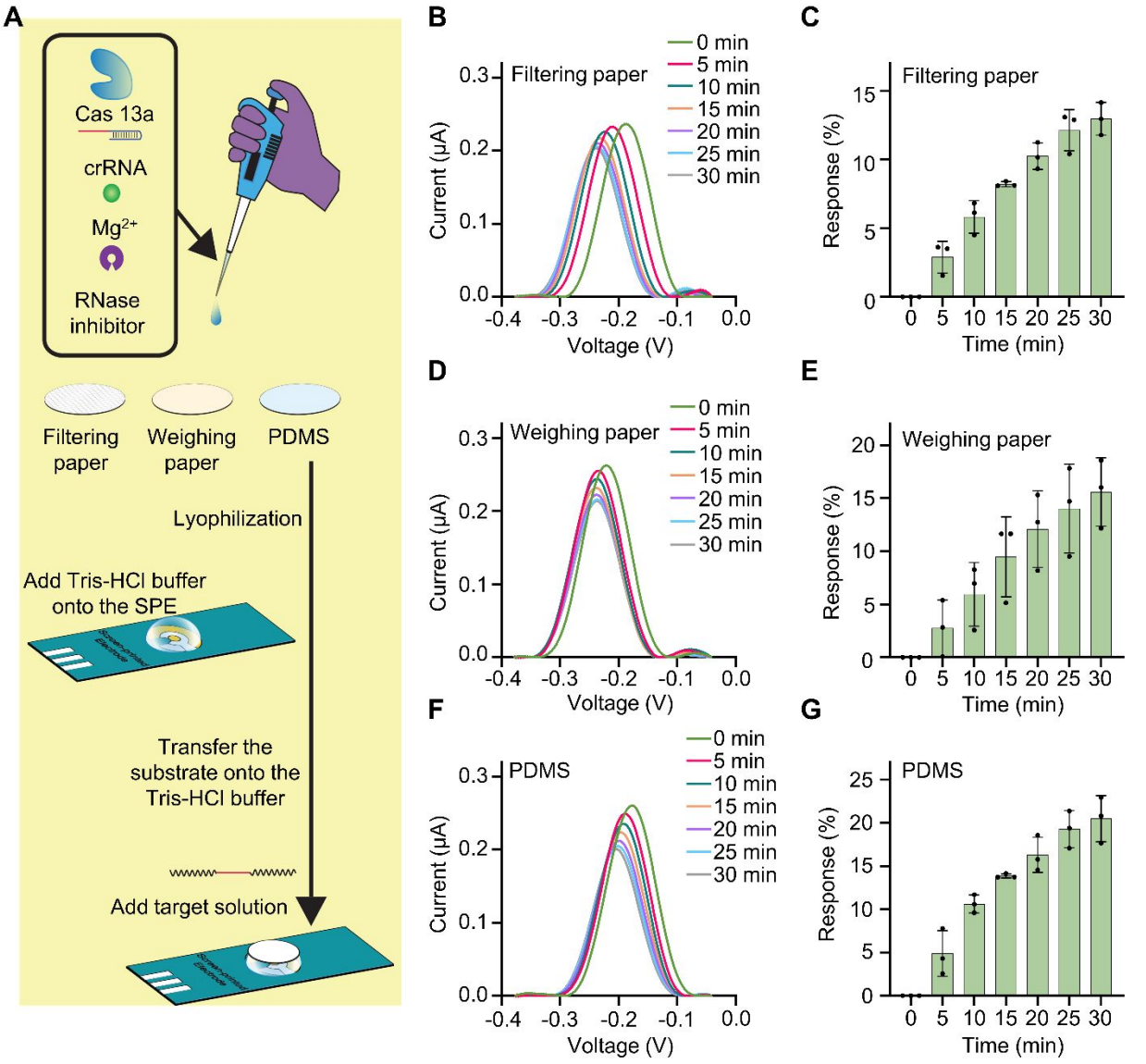

Figure 4. Effect of lyophilization substrate materials on the detection. (A) Workflow of CRISPR assay lyophilization and rehydration. The reagents were first lyophilized on filter paper, weighing paper and PDMS, and then rehydrated in a target-spiked Tris buffer solution on screen-printed electrodes. (B, D, F) Representative time-sequential SWV scans after rehydration of lyophilized substrates of (B) filter paper, (D) weighing paper, and (F) a PDMS membrane. (C, E, G) Relative peak current changes over 30 min for lyophilization substrates of (C) filter paper, (E) weighing paper, and (G) a PDMS membrane (n = 3).

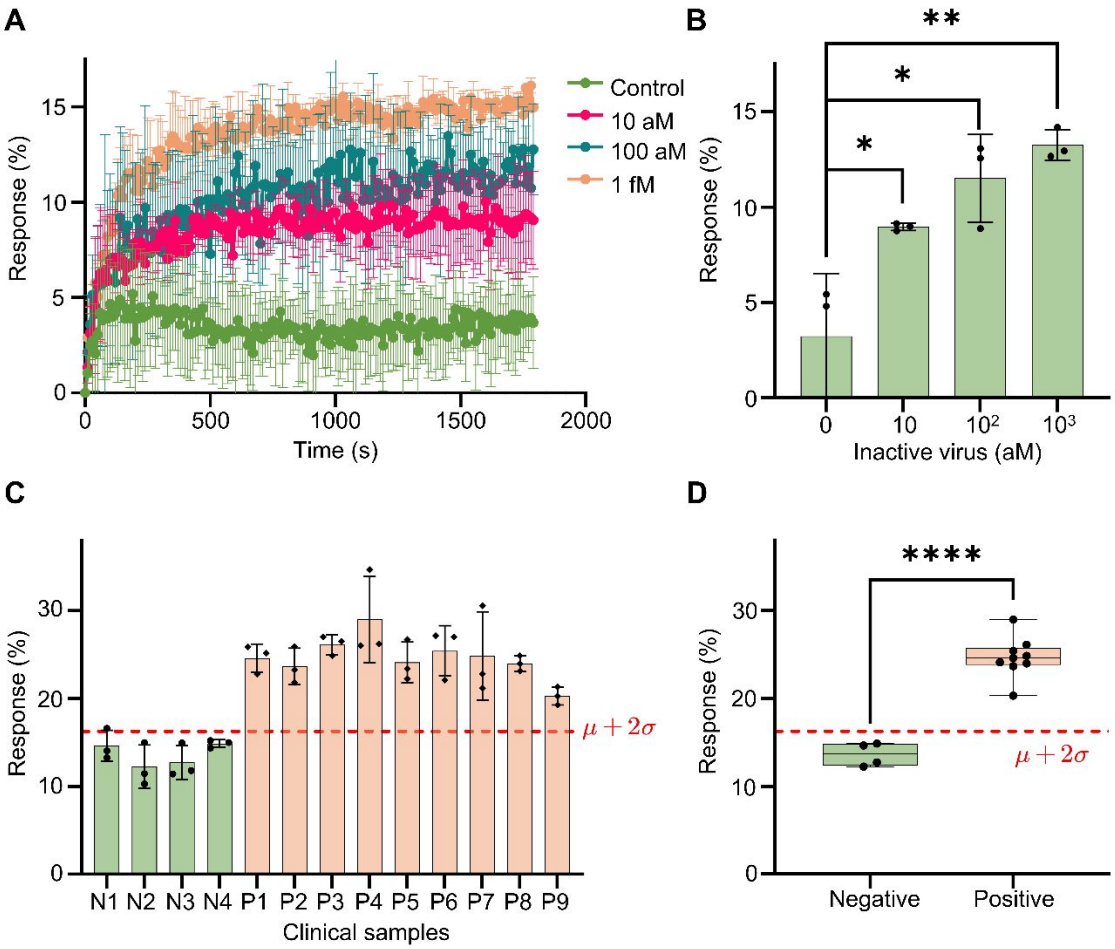

Figure 5. Device validation using heat-inactivated and clinical SARS-CoV-2 samples. (A) The change in SWV peak current recorded at a 10 s interval for 30 min, with different concentrations of heat-inactivated SARS-CoV-2 samples (n=3). (B) The change in SWV peak current after 10 min reaction, with different concentrations of heat inactivated SARS-CoV-2 (n = 3; *, $P < 0.05$; **, $P < 0.01$). (C) The relative change in SWV peak current after 10 min reaction, with four negative and nine positive clinical samples (n = 3). The cutoff threshold (16.27%) was set to be mean response from negative samples plus two standard deviations. (D) Box plot of SWV peak current change for negative and positive clinical samples, calculated from the mean value of three replicates for each individual sample. The hinges represent the first and third quartiles of the

responses. Student's t-test was performed to determine the statistical differences between the negative and positive samples. ($n \geq 4$; ****, $P < 0.0001$)

Table 1. Comparison of the point-of-care device reported in this work with state-of-the-art technologies.

	This work	CRISPR-gFET[21]	CRISPR-chip[51]	CRISPR-mobile phone mictoscope[52]	STOPCovid[20], [53]	DETECTR[46]
Sample-to-result	25 min	45 min	N/A	75 min	70-80 min	40 min
Limit of detection (LOD)	10 aM	1 aM	1.7 fM	0.166 fM	2.2-11.2 aM (with amplification)	16.6 aM (with amplification)
Amplification	No need	No need	No need	No need	RT-LAMP (60 min)	RT-LAMP (20-30 min)
Sample treatment	10 min (Thermal lysis)	5 min (Thermochemical lysis)	N/A (Extraction and isolation)	45 min (Extraction and isolation)	5-10 min (Thermochemical lysis)	10 min (Extraction and isolation)
CRISPR reaction	10 min (Engineered LwaCas13a)	30 min (LwaCas13a)	15 min (dCas9)	30 min (LbuCas13a)	N/A (AapCas12b)	10 min (LbCas12a)
Instrument	Smart phone-potentiostat	Semiconductor analyzer; heating block	Heating block; Potentiostats; DNA extraction setup	Mobile phone-fluorescence reader; RNA extraction setup	Heating block; plate reader	Heating block; plate reader or lateral flow strip
Point-of-care	Yes	No	No	No	Yes	No

N/A: not available